



OPEN ACCESS

EDITED BY

He Liu,
Jilin University, China

REVIEWED BY

Jinshan Guo,
Southern Medical University, China
Bo Lu,
Wuhan University of Technology, China
Chengcheng Yin,
China Medical University, China
Fu Yin Hsu,
National Taiwan Ocean University,
Taiwan

*CORRESPONDENCE

Zhihua Li,
lizhuhua@ncu.edu.cn
Junchao Wei,
weijunchao@ncu.edu.cn

SPECIALTY SECTION

This article was submitted to
Biomaterials,
a section of the journal
Frontiers in Bioengineering and
Biotechnology

RECEIVED 15 July 2022

ACCEPTED 13 September 2022

PUBLISHED 05 October 2022

CITATION

Yao H, Luo J, Deng Y, Li Z and Wei J
(2022), Alginate-modified mesoporous
bioactive glass and its drug delivery,
bioactivity, and osteogenic properties.
Front. Bioeng. Biotechnol. 10:994925.
doi: 10.3389/fbioe.2022.994925

COPYRIGHT

© 2022 Yao, Luo, Deng, Li and Wei. This
is an open-access article distributed
under the terms of the [Creative
Commons Attribution License \(CC BY\)](#).
The use, distribution or reproduction in
other forums is permitted, provided the
original author(s) and the copyright
owner(s) are credited and that the
original publication in this journal is
cited, in accordance with accepted
academic practice. No use, distribution
or reproduction is permitted which does
not comply with these terms.

Alginate-modified mesoporous bioactive glass and its drug delivery, bioactivity, and osteogenic properties

Haiyan Yao^{1,2,3}, Jun Luo^{1,3,4}, Yunyun Deng^{1,3}, Zhihua Li^{1,3,4*} and Junchao Wei^{1,2,3,4*}

¹School of Stomatology, Nanchang University, Nanchang, China, ²College of Chemistry, Nanchang University, Nanchang, China, ³Jiangxi Province Key Laboratory of Oral Biomedicine, Nanchang, China, ⁴Jiangxi Province Clinical Research Center for Oral Disease, Nanchang, China

Mesoporous bioactive glass (MBG) is widely used in bone tissue repairing and drug loading. However, burst release of drug and poor compatibility with other materials limited its application. It is an effective way to modify MBG with a polymer brush to improve the properties. Herein, an alginate-modified MBG was prepared, and then, the effects of ALG on the properties of MBG were investigated. The results demonstrate that ALG could improve the drug loading efficiency, prolong drug release times, and make orderly deposition of apatite on the surface of MBG. Furthermore, MBG@ALG significantly promoted the osteogenic differentiation of MC3T3-E1 cells, demonstrating that surface modification of MBG by ALG can improve its properties, which will further broaden the application of MBG in tissue engineering.

KEYWORDS

mesoporous bioactive glass, surface modification, alginate, drug loading, bone regeneration

1 Introduction

Bioactive glass (BG) is widely used in bone tissue engineering scaffold (Vallet-Regi and Salinas, 2021) and polymer composites for bone regeneration (Zhao et al., 2021) due to its excellent biocompatibility and osteogenic properties. Mesoporous bioactive glass (MBG) not only possesses the advantages of BG but also showed superior *in vitro* bone-forming bioactivities (Rahaman et al., 2011; Schumacher et al., 2021), high porosity, and specific surface area. Therefore, MBG has been widely used as a drug delivery system (Lopez-Noriega et al., 2010) for the treatment of bone tissue diseases; for example, various functional molecules, such as small molecule drugs (alendronate) (Ravanbakhsh et al., 2019) and growth factors (BMP-2, VEGF) have been loaded into MBG (Kim et al., 2016; Schumacher et al., 2017). However, the poor binding ability with other materials (Kargozar et al., 2019), burst release of drugs, and easy formation of protein crowns in biological media (Pontremoli et al., 2020; Sharifi et al., 2022) have limited the application of MBG. Therefore, it is of much importance to tailor the properties of MBG to improve its applications.

The surface of nanomaterials play critical roles in many physical and chemical processes, while the surface ligands or molecules binding to the surface are essential components of nanomaterials and affect its interactions with other materials or biological systems (Kango et al., 2013; Boles et al., 2016), and thus many works have been carried out to tune the surface of nanomaterials with organic ligands and polymer brushes (Boles et al., 2016; Heinz et al., 2017). As for MBG, the surface molecules or polymer brushes may work as gatekeepers and tune its drug delivery ability, for example, various molecules, such as 3-aminopropyltrimethoxysilane (Wang et al., 2018) and poly-L-glutamic acid (Das et al., 2021) have been used to enhance its drug loading efficiency and prolong the drug release time. In addition, the surface polymer brushes may have great effect on the bioactivity of MBG (Kargozar et al., 2019), which will greatly affect the biomineralization of the apatite and the binding ability of MBG to tissues. For example, poly (amidoamine) (PAMAM) dendrimer-coated mesoporous bioactive glass nanoparticles (MBG) (PAMAM@MBG) were prepared and used for treatment of dentine hypersensitivity (Bae et al., 2019), while the results demonstrated that the PAMAM@MBG had excellent mineralization ability and showed a better occluding effect for dentinal tubules than that of MBG. In addition, the surface modification of nanomaterials improves the phase compatibility between nanomaterials and polymer matrix, and thus improves the mechanical properties of polymer composites (Kango et al., 2013). For instance, polydopamine has been coated on the surface of MBG, which greatly improves the mechanical properties of MBG/PLLA scaffolds (Xu et al., 2018). Generally, it has been an effective method to graft polymers or organic molecules on the surface of MBG to improve its charming properties. However, it is still a great challenge to modify the surface of MBG with mild conditions and improve multiple performances of MBG simultaneously.

Alginate (ALG) is an anionic polymer with good biocompatibility and low toxicity, and has been widely applied in biomedical applications (Lee and Moone, 2012). ALG can be tethered on the surface of nanomaterials to improve the colloidal stability of various nanobuilding blocks. For example, ALG-modified SiO₂ (Yan et al., 2019), carbon nanotubes (Yao et al., 2021), and upconversion nanoparticles (Cao et al., 2020) show good colloidal stability and biocompatibility. Furthermore, the ALG molecules can also reduce protein adsorption to nanomaterials and inhibit the formation of protein crowns. Mooney's group prepared cysteine-functionalized ALG--derived polymers as stabilizers to coat the surface of gold nanoparticles (GNPs), which increase the stability of the GNPs and reduce the adsorption of proteins on GNPs (Kodiyani et al., 2012). In addition, ALG has immunomodulatory effect, which can accelerate the wound healing by promoting the anti-inflammatory polarization of macrophages (Bygd and Bratlie, 2016; Kerschenmeyer et al.,

2017). In addition, the ALG polymers contain multiple reactive groups, such as hydroxyl and carboxyl groups, which could be an ideal candidate for the further functionalization of materials with special functions, for example, cell targeting ligands and therapeutic drugs (Ahmad Raus et al., 2021). Therefore, it is definite that ALG as a polymer brush can greatly alter the biological properties of nanomaterials. Herein, if ALG was combined with MBG, the advantages of both the materials may have synergistic effect and realize the improvements of the multifunction of MBG.

In this work, ALG was grafted on MBG (MBG@ALG) *via* a simple method (Figure 1), and all the reactions were conducted at mild temperature and no toxic solvents were used. In addition, the method is universal and can be used to modify the surface of other kinds of nanomaterials and improve their properties. In addition, the effect of ALG on drug loading efficiency, bioactivity, biocompatibility, and osteogenic properties of MBG were investigated. The results demonstrated that ALG brush can enhance drug loading efficiency, prolong drug release time, promote the orderly deposition of apatite, and improve osteogenic performance of MBG, having a positive effect to improve the performance of MBG and broaden its application in bone tissue engineering.

2 Materials and methods

2.1 Materials

Hexadecyl trimethyl ammonium bromide (CTAB, 98%), tetraethyl orthosilicate (TEOS), triethyl phosphate (TEP), calcium nitrate tetrahydrate (Ca(NO₃)₂·4H₂O), ammonium hydroxide (NH₃·H₂O), and ethanol were purchased from Sinopharm Chemical Reagent Co., Ltd. (Shanghai, China). Sodium alginate (ALG, the viscosity of ALG (1%, Brookfield LV, 20°C) is 350–550 cP), 3-aminopropyltrimethoxysilane (APTES), ethyl-3-(3-dimethylaminopropyl) carbodiimide hydrochloride (EDC), N-hydroxysuccinimide (NHS, 98%), and sodium alginate (98%) were purchased from Aladdin Scientific Co., Ltd. (Shanghai, China). Acridine orange/ethidium bromide was purchased from BestBio Co., Ltd. (Shanghai, China). The MTT kit and Alkaline Phosphatase Color Development Kit were purchased from Beyotime Co., Ltd. (Shanghai, China). Alizarin Red S (ARS) staining was purchased from Solarbio Co., Ltd. (Beijing, China).

2.2 Methods

2.2.1 Preparation of MBG@ALG

First, MBG was synthesized by a reported method (Ravanbakhsh et al., 2019). Briefly, 0.7 g of CTAB was dissolved in 33 ml of water under stirring, and then 10 ml of

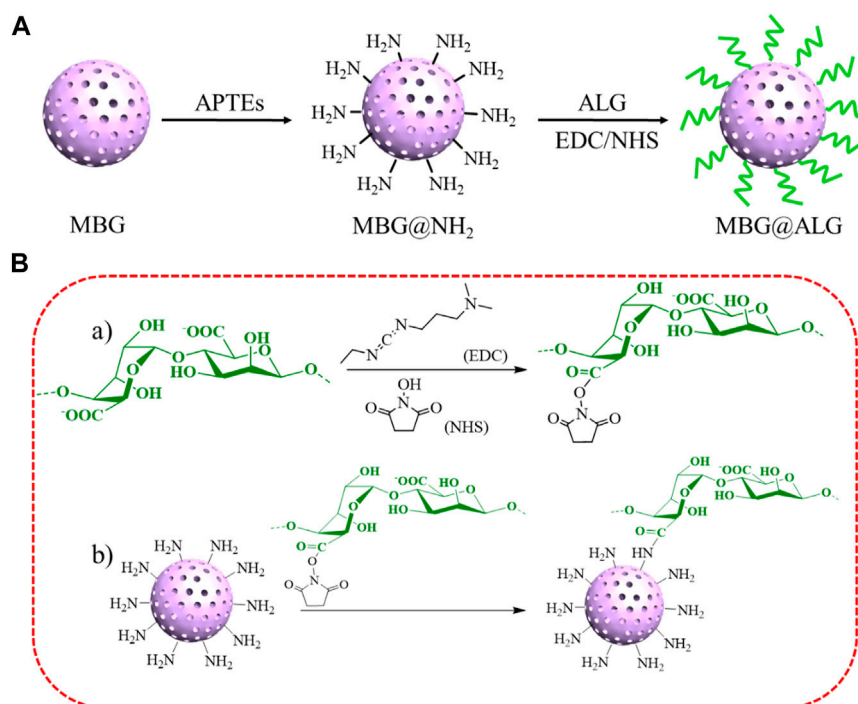


FIGURE 1
Schematic illustration of the construction of MBG@ALG (A) and reaction scheme (B).

ethyl acetate was added. 30 min later, 7 ml of aqueous ammonia (3 mol. L^{-1}) was added. 15 min later, 3.6 ml of TEOS, 0.36 ml of TEP, and 2.277 g of $\text{Ca}(\text{NO}_3)_2 \cdot 4\text{H}_2\text{O}$ were sequentially added to the abovementioned mixture at every 30 min interval. The solution was vigorously stirred for another 4 h, the precipitate was collected by centrifugation, and then washed three times with ethanol and water in turn. The raw product was dried at 60°C for 24 h and then calcined at 650°C for 6 h to obtain MBG.

Second, 0.3 g of MBG and 0.6 ml of APTES were added in 100 ml of ethanol, and then the mixed solution was refluxed at 80°C for 24 h. The precipitate was collected by centrifugation, washed three times with ultrapure water, and freeze-dried to obtain MBG@ NH_2 .

Third, 0.25 g of ALG was dissolved in 50 ml of water and stirred for 24 h, then 0.2399 g of EDC and 0.1439 g of NHS were added in the solution and stirred for 2 h. 0.25 g of MBG@ NH_2 was added in the abovementioned solution and stirred for 24 h and then centrifuged and washed with deionized water and lyophilized.

2.2.2 Characterization

The weight loss of different samples was measured by using a thermal gravimetric analyzer (TGA, Perkin Elmer, TGA 4000, United States). The crystalline structure was measured on X-ray diffraction (XRD, SmartLab 9 KW, Japan). The morphology of different samples was observed using a transmission electron microscope (TEM, JEOL, JEM-2100, Japan) and scanning

electron microscope (SEM, Thermo Fisher Scientific, Apero C HiVac, United States).

2.2.3 Drug loading and release

Simvastatin (SIM) was used as a model drug. Briefly, 10 mg of MBG and MBG@ALG was dispersed in 10 ml of ethanol, and 5 mg of SIM was added and stirred for 24 h, respectively. Then, the supernatant was centrifuged and the absorbance value at 238 nm of the supernatant was measured. The mass of SIM in the supernatant was calculated using the measured SIM standard curve. The loading efficiency (%) and drug content (%) were calculated using the following formula:

$$\text{Loading efficiency (\%)} = (\text{weight of drug in MBG}/\text{initial weight of drug}) \times 100\%$$

$$\text{Drug content (\%)} = (\text{weight of drug in MBG}/\text{weight of MBG}) \times 100\%$$

in vitro drug release of SIM from MBG and MBG@ALG was performed by the dialysis bag diffusion method. 2 mg of MBG and MBG@ALG loaded with SIM was suspended in 2 ml of phosphate-buffered saline (PBS, pH7.4) and introduced into the dialysis bag. The dialysis bag was kept at 30 ml of PBS containing 20% ethanol and transferred to constant temperature shaker. At each time point (1, 3, 12, 24, 24, 48, and 96 h), 2 ml of the release medium was taken out and replaced with equal amounts of fresh medium. The amount of released SIM was evaluated by ultraviolet-visible (UV) analysis at a wavelength of 238 nm.

2.2.4 Bioactivity test in simulated body fluids

An SBF (simulated body fluid) solution was first prepared according a reported method (Kokubo and Takadama, 2006), and then 20 mg of MBG and MBG@ALG powder were soaked in 20 ml of SBF at 37°C for 7 days in a shaking incubator. The SBF was refreshed every 24 h. Then, SEM was conducted to evaluate apatite formation.

2.2.5 Biocompatibility test

The samples were irradiated under UV for 2 h, and then added into a culture medium. The concentration was diluted with a culture medium to 500, 250, 125, 50, and 25 µg/ml 100 µl of the culture medium containing MC3T3-E1 cells at a density of 8×10^4 cells/mL were seeded into a 96-well plate and incubated for 24 h for cell attachment. Subsequently, the culture media was replaced with 100 µl of materials at concentrations of 500, 250, 125, 50, and 25 µg/ml. After the cells were coincubated with nanoparticles for 24 h, the medium was sucked out and PBS was added for washing several times, then the MTT reagent (10 µl) mixed with 100 µl of fresh medium was added to each well. After 4 h of incubation, the medium was removed and 150 µl of DMSO was added to fully dissolve the formazan, and then the OD value at 490 nm was measured.

AO/EB (Acridine Orange/Ethidium Brmide) staining was used to further detect the apoptosis of MC3T3-E1 cells. 100 µl of culture media containing MC3T3-E1 cells at a density of 8×10^4 cells/mL were seeded into a 96 plate and incubated at 37°C under atmosphere of 5% CO₂ for 24 h. Subsequently, the culture media was replaced with 100 µl of fresh medium containing samples at various concentrations of 500, 250, 125 µg/ml. After 24 h co-incubation, fresh medium was used to wash each well several times, and then AO/EB reagent was added to each well for 30 s. Finally, the survival of cells was observed by fluorescence microscopy.

2.2.6 Osteogenesis differentiation

100 µl of culture media containing MC3T3-E1 cells at a density of 1×10^4 cells/mL were seeded into a 96-well plate and incubated at 37°C under atmosphere of 5% CO₂ for 24 h. Subsequently, the culture media was replaced with 100 µl of medium containing samples at concentrations of 250 µg/ml. After 7 and 14 days, PBS was used to wash the plate several times, and the cells were fixed with 4% paraformaldehyde for 30 min. Then, the cells were stained with Alkaline Phosphatase (ALP) Color Development Kit and Alizarin Red S (ARS) Staining.

3 Results and discussion

3.1 Characterization of different samples

MBG was spherical, mono-dispersed, and porous particles (Figures 2A,B), the diameter of MBG was 222 ± 19 nm (Figure 2C). When ALG was grafted on the surface of MBG,

a polymer coating could be clearly observed on the surface of MBG (Figures 2D,E), and the mean diameter of the MBG@ALG was 232 ± 22 nm (Figure 2F), which demonstrated that ALG was successfully grafted onto the MBG surface.

In the FT-IR spectrum of MBG, the peaks at $1,080 \text{ cm}^{-1}$, 806 cm^{-1} , and $1,633 \text{ cm}^{-1}$ (Figure 3A) were ascribed to Si–O–Si, O–Si–O, and Si–OH bands, respectively (Yan et al., 2017). For the spectrum of MBG@ALG, a new peak located at 944 cm^{-1} was corresponded to the C–O stretching, which was derived from ALG (Ding et al., 2021), demonstrating that ALG was successfully anchored onto MBG. The XRD patterns displays a wide-angle diffraction peak centered at $2\theta = 20.4^\circ$, which was attributed to the amorphous nature of pristine MBG. After ALG was grafted, the wide-angle diffraction peak did not change, which is in consistence with the pattern of MBG (Figure 3B), demonstrating that the original crystalline structure of MBG remains unaltered after ALG surface modification. The TGA results showed that the weight loss of MBG@ALG was 24.7%, which consist of 5.2% weight loss of absorbed solvent before 150°C and 19.5% weight loss of the ALG between 150 and 800°C (Figure 3C). The 13.4% weight loss of MBG was due to the absorption of the solvent. The results show that the ALG coating was successfully prepared on the MBG surface.

The N₂ adsorption isotherms and pore size distribution of MBG, MBG@NH₂, and MBG@ALG demonstrated the characteristic of mesoporous (Figure 4). The surface area, pore volume, and pore diameter of MBG were 196 m²/g, 0.55 cm³/g, and 11.3 nm (Table 1), respectively. After being treated with APTES, the surface area, pore volume, and pore diameter showed some changes, and the corresponding results of MBG@NH₂ were found to be 171 m²/g, 0.458 cm³/g, and 10.7nm, respectively. When ALG polymer chains were grated with MBG@NH₂, evident changes of the surface area, pore volume, and pore diameter of MBG@ALG were found, and the results were 162 m²/g, 0.427 cm³/g, and 10.5 nm (Table 1), respectively, much smaller than that of MBG, further demonstrating that ALG was successfully grafted on the surface and have an evident affection on its physical properties.

3.2 Drug loading and release assays

The surface can significantly alter the drug loading efficiency and the drugs release time, and various surface molecules are found to be very useful for improving drug delivery (Cui et al., 2020). SIM was selected as a model drug, the loading efficiency of MBG was 24.5% (Xiao et al., 2019a; Xiao et al., 2019b). After ALG polymer chains were grated on the MBG, the loading efficiency was found to be improved, and the result was 31.2% (Figure 5A). The drug content of MBG and MBG@ALG was 12.2% and 15.6%, respectively (Figure 5B). The results demonstrated that ALG polymer chains can significantly improve the drug loading efficiency of MBG.

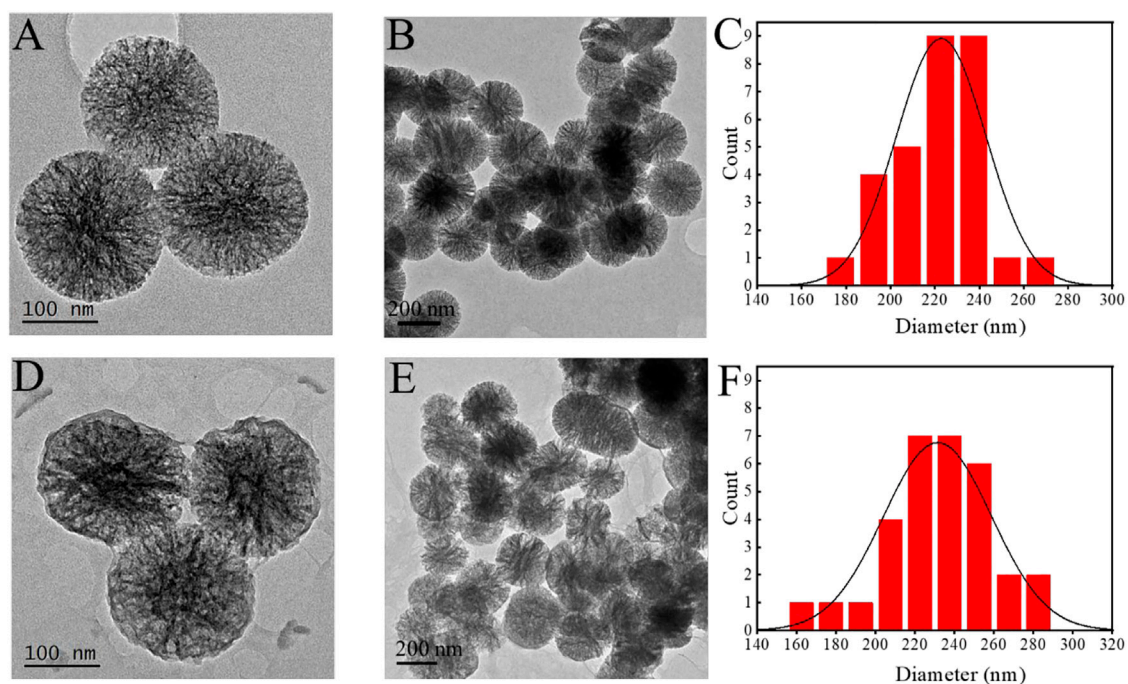


FIGURE 2
TEM images of MBG (A,B) and MBG@ALG (D,E). Particle size analysis of MBG (C) and MBG@ALG (F).

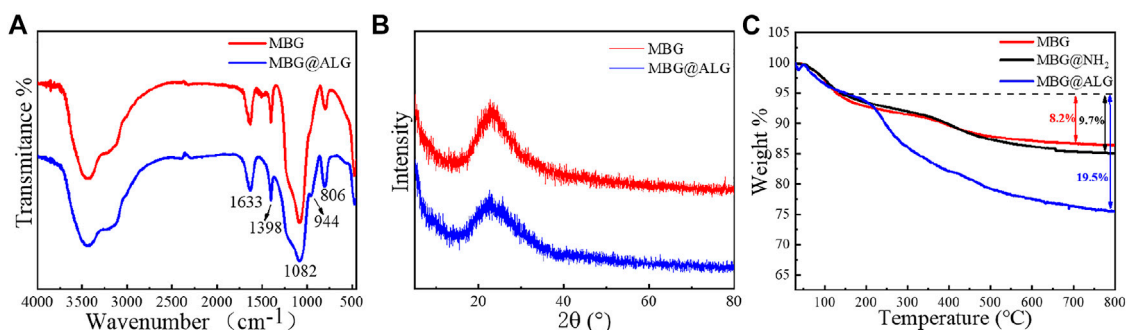


FIGURE 3
(A) FTIR spectra of MBG and MBG@ALG, (B) XRD patterns of MBG and MBG@ALG, and (C) TGA curve of MBG, MBG@NH₂, and MBG@ALG.

The drug release curves of MBG and MBG@ALG can be divided into three stages (Figure 5C). In the first stage, a burst release could be observed in the curves of MBG and MBG@ALG, which can be ascribed to the adsorbed SIM on the surface of MBG and MBG@ALG, rapidly diffusing into the solution. In the second stage, the release velocity of the SIM was significantly lower than that of the first stage, while this period of drug release is resulted from the SIM molecules which have entered the mesoporous channel, and therefore it takes a long time for the drug molecules to diffuse into the solution. However, when

compared with the drug release curves in the second stage, it can be found that the release rate of SIM from MBG is faster than that of MBG@ALG. This is because the ALG polymer chains on the surface of MBG@ALG can hinder the diffusion of the SIM. In the third stage (after 48 h), the drug release rate decays to nearly zero, which means that, in this stage the drug diffusion and drug adsorption is dynamically balanced.

Furthermore, as shown in Figure 5C, in the second stage, there was an evident linear region both in the curves of MBG and MBG@ALG (shown in the rectangle), the drug release rate is

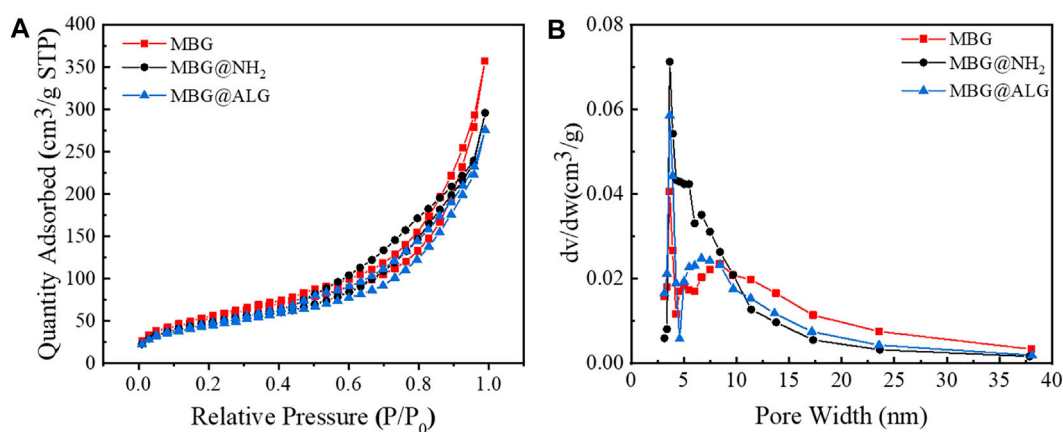


FIGURE 4
N₂ adsorption–desorption isotherms (A) and pore-size distribution (B) of MBG, MBG@NH₂, and MBG@ALG.

TABLE 1 Summary of the including specific surface area, pore volume, and pore size as determined from N₂ adsorption–desorption isotherms.

| Sample | Specific surface area (m ² /g) | Pore volume (cm ³ /g) | Pore size (nm) |
|---------------------|---|----------------------------------|----------------|
| MBG | 196 | 0.552 | 11.3 |
| MBG@NH ₂ | 171 | 0.458 | 10.7 |
| MBG@ALG | 162 | 0.427 | 10.5 |

linear with time, which is consistent with the zero-order kinetics (Marcos Luciano, 2015). In addition, on considering the porous structure of MBG and MBG@ALG, we try to use the Higuchi model to describe the release of SIM, the relationship between drug release amount and the square root of time was calculated and shown in Figure 5D, showing linear relationships and equations, implying that the release profiles can be explained *via* the Higuchi model, and this result is also consistent with the published work about MBG (Xiao et al., 2019a; Zhu and Stefan, 2019). All these results may demonstrate that ALG modification can improve the drug loading efficiency of MBG and prolong the drug release time without affecting its release mechanism.

3.3 *In vitro* bioactivity

The surface ligands have great influence on mineral deposition, such as defining the mineral-deposition site and affecting the morphology of apatite (Meldrum F, 2008; Gordon and Joester, 2011). The SEM images showed both MBG and MBG@ALG are spherical nanoparticles with a particle size of about 200 nm (Figures 6A,B). After treated in SBF, many irregular apatite plates are formed around MBG (Figure 6C), which may be that the

released Ca²⁺ increases the concentration of Ca²⁺ around MBG, inducing nucleation and the growth of apatite. Generally, due to the biodegradation ability of MBG, when the MBG samples were immersed into the SBF solution, the mineralization behaviors also happens and this may be a dissolve-regrowth scheme. After the ALG polymer chains were grafted on MBG, compared with MBG that treated with SBF for 7 days, a regular and tightly arranged plate structure can be observed on the surface of the MBG@ALG (Figure 6D). Since SBF were used as a mineralization medium, the ALG can chelate Ca²⁺ from the solution and induce nucleation as crystal seed, therefore, orderly growth of apatite on the surface of MBG@ALG formed, in addition, the amount of plate apatite of MBG@ALG (Figure 6D) is much more than that of MBG (Figure 6C), demonstrating that grafting of ALG can control the morphology and accelerate the mineralization of apatite, which may broaden the application of MBG in bone tissue engineering.

3.4 Biocompatibility test of MBG and MBG@ALG

MBG and MBG@ALG show excellent biocompatibility, even when the concentration of the materials reached to 500 µg/ml.

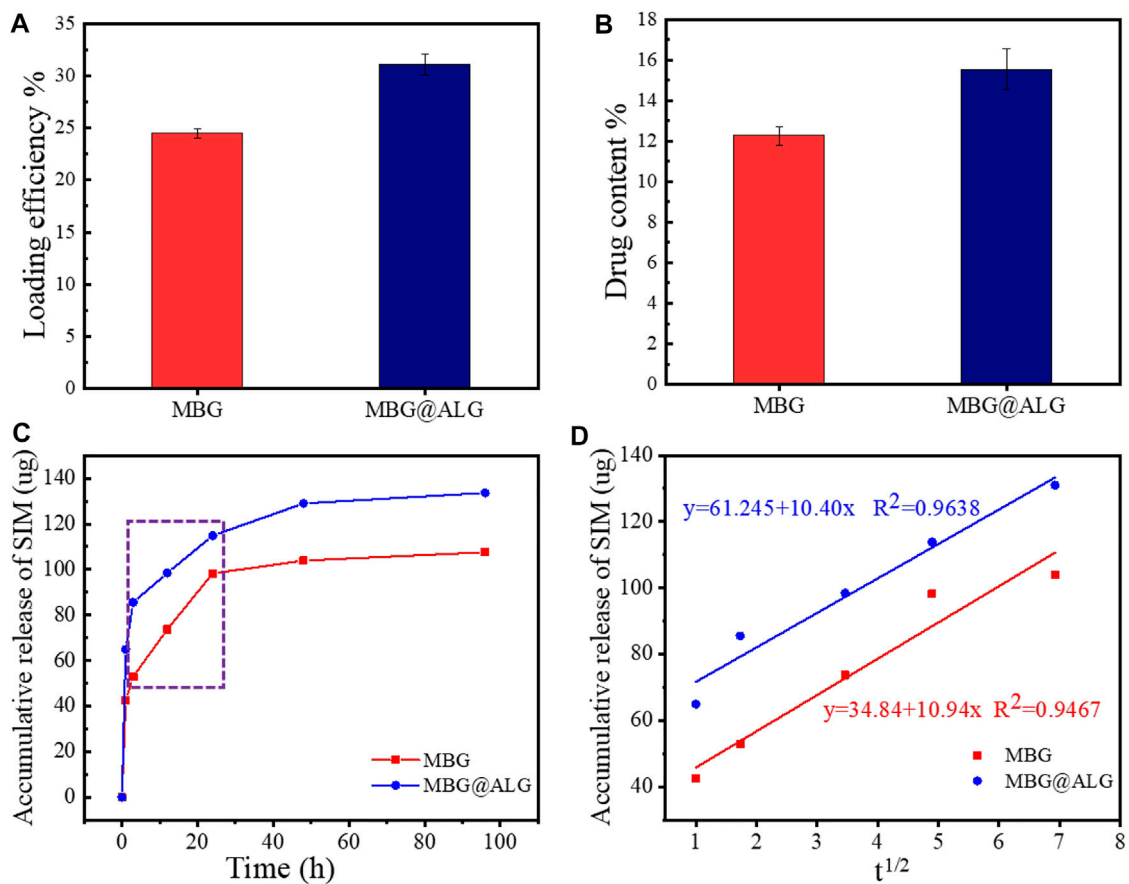


FIGURE 5 (A) Loading efficiency of MBG and MBG@ALG, (B) drug content of MBG and MBG@ALG, (C) release curves of MBG and MBG@ALG, and (D) the linear relationship between drug release and the square root of release time at the Higuchi model release phase.

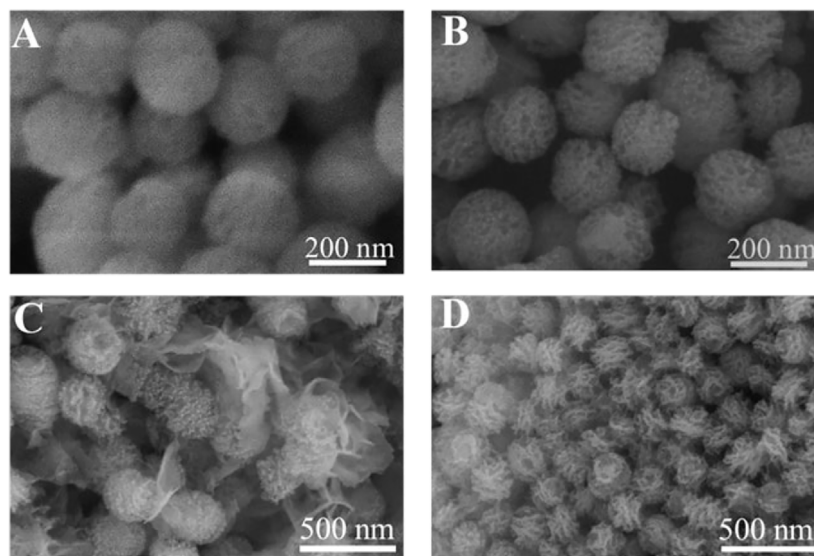
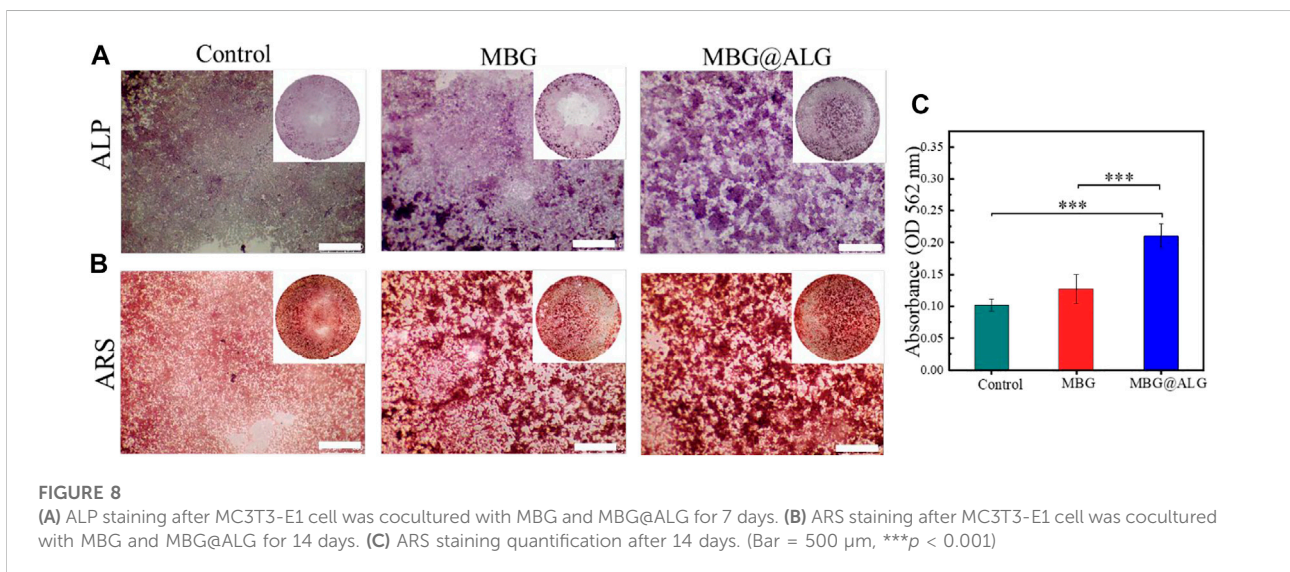
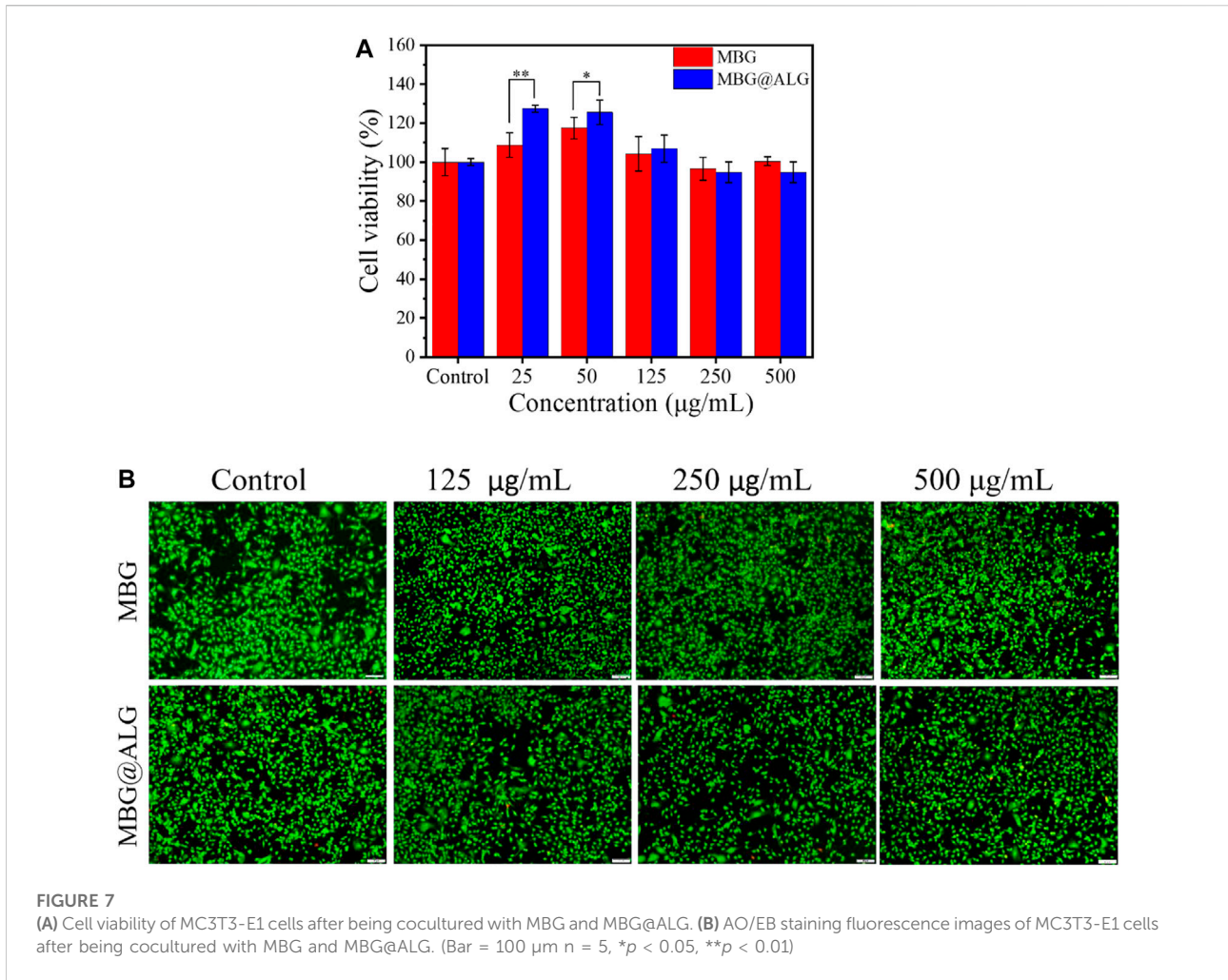


FIGURE 6 SEM image of MBG (A) and MBG@ALG (B). SEM image of MBG (C) and MBG@ALG (D) after treated with SBF for 7 days.



When the concentration was 25 $\mu\text{g/ml}$, the cell viability of MBG and MBG@ALG was 108% and 127%, respectively. At the concentration of 50 $\mu\text{g/ml}$, the cell viability of MBG and MBG@ALG was 117% and 125% (Figure 7A), respectively. These indicate that MBG and MBG@ALG can significantly promote cell proliferation at low concentrations, and the cell viability of MBG@ALG is significantly higher than that of MBG at the same concentration. When the concentration of MBG was 100, 250, and 500 $\mu\text{g/ml}$, the cell viability was 104%, 96%, and 100%, respectively. When the concentration of MBG@ALG was 100, 250, and 500 $\mu\text{g/ml}$, the cell viability was 107%, 94%, and 95%, respectively (Figure 7A). MBG and MBG@ALG showed good compatibility at these concentrations, and the effects of MBG and MBG@ALG on cell viability at these concentrations were not significantly different.

AO/EB staining further verified the excellent biocompatibility of MBG@ALG (Figure 7B). The cells survived well after being cocultured with the material (green fluorescence), with only a few apoptotic cells (red fluorescence). These results of MBG@ALG was biocompatible and can promote cell proliferation at low concentrations.

3.5 Osteogenesis differentiation of MC3T3-E1 cells

MBG has good osteoconductivity and osteoinductive properties, which can promote the osteogenic differentiation of cells. ALP, an early marker of osteogenic differentiation and mineralized nodules—a late marker of osteogenic differentiation, were detected by ALP staining and ARS staining, respectively. After the cells were cocultured with the MBG and MBG@ALG for 7 days, respectively, the purple color in the MBG@ALG group was significantly stronger than that in the MBG group (Figure 8A), indicating that the cells in the MBG@ALG group expressed more ALP. This result demonstrated that MBG@ALG has a great effect on promoting the early osteogenic differentiation of MC3T3-E1 cells. After 14 days of coculture, the ARS staining images and quantification data showed that the number and density of mineralized nodules in the MBG@ALG group were higher than those in the MBG group (Figures 8B,C), indicating that MBG@ALG had an excellent effect on promoting extracellular matrix mineralization. These results demonstrate that the surface modification of ALG promotes both early osteogenic differentiation and late osteoblast maturation, which will further broaden the application of MBG.

4 Conclusion

In this work, an ALG-modified MBG was successfully prepared (MBG@ALG), while the ALG chains on the

surface of MBG could improve the drug loading efficiency and restrain the drug release speed. Furthermore, MBG@ALG showed excellent biocompatibility and could promote the osteogenic differentiation of cells, demonstrating that the surface functionalization of MBG with ALG has a significant impact on its properties, which may promote the further application of MBG in drug delivery and bone tissue engineering.

Data availability statement

The raw data supporting the conclusion of this article will be made available by the authors, without undue reservation.

Author contributions

HY: investigation, methodology, and writing original draft. JL: conceptualization. YD: methodology. ZL: project administration. JW: conceptualization, project administration, and writing—review and editing.

Funding

This work was supported by the financial support from the National Natural Science Foundation of China (Nos. 52163016 and 81960205), Jiangxi Provincial program for the academic and technological leaders of main subjects (20213BCJL22051), and Jiangxi Key Research and Development Program (20202BBG73012).

Conflict of interest

The authors declare that the research was conducted in the absence of any commercial or financial relationships that could be construed as a potential conflict of interest.

Publisher's note

All claims expressed in this article are solely those of the authors and do not necessarily represent those of their affiliated organizations, or those of the publisher, the editors, and the reviewers. Any product that may be evaluated in this article, or claim that may be made by its manufacturer, is not guaranteed or endorsed by the publisher.

References

- Ahmad Raus, R., Wan Nawawi, W. M. F., and Nasaruddin, R. R. (2021). Alginate and alginate composites for biomedical applications. *Asian J. Pharm. Sci.* 16, 280–306. doi:10.1016/j.ajps.2020.10.001
- Bae, J., Son, W. S., Yoo, K. H., Yoon, S. Y., Bae, M. K., Lee, D. J., et al. (2019). Effects of poly(amidoamine) dendrimer-coated mesoporous bioactive glass nanoparticles on dentin remineralization. *Nanomaterials* 9, 591. doi:10.3390/nano9040591
- Boles, M. A., Ling, D., Hyeon, T., and Talapin, D. V. (2016). Erratum: The surface science of nanocrystals. *Nat. Mat.* 15, 364. doi:10.1038/nmat4578
- Bygd, H. C., and Bratlie, K. M. (2016). The effect of chemically modified alginates on macrophage phenotype and biomolecule transport. *J. Biomed. Mat. Res. A* 104, 1707–1719. doi:10.1002/jbm.a.35700
- Cao, C., Hong, C., Li, Y., Li, G., and Jiang, G. (2020). A long-term and stable surface modification method for lanthanide doped upconversion nanoparticles by oxidized alginate. *Z. Anorg. Allg. Chem.* 646, 1607–1610. doi:10.1002/zaac.202000262
- Cui, L., Zhang, J., Zou, J., Yang, X., Guo, H., Tian, H., et al. (2020). Electroactive composite scaffold with locally expressed osteoinductive factor for synergistic bone repair upon electrical stimulation. *Biomaterials* 230, 119617. doi:10.1016/j.biomaterials.2019.119617
- Das, M. P., Pandey, G., Neppolian, B., and Das, J. (2021). Design of poly-L-glutamic acid embedded mesoporous bioactive glass nanospheres for pH-stimulated chemotherapeutic drug delivery and antibacterial susceptibility. *Colloids Surfaces B Biointerfaces* 202, 111700. doi:10.1016/j.colsurfb.2021.111700
- Ding, X., Shi, J., Wei, J., Li, Y., Wu, X., Zhang, Y., et al. (2021). A biopolymer hydrogel electrostatically reinforced by amino-functionalized bioactive glass for accelerated bone regeneration. *Sci. Adv.* 7, eabj7857. doi:10.1126/sciadv.abj7857
- Gordon, L. M., and Joester, D. (2011). Nanoscale chemical tomography of buried organic-inorganic interfaces in the chiton tooth. *Nature* 469, 194–197. doi:10.1038/nature09686
- Heinz, H., Pramanik, C., Heinz, O., Ding, Y., Mishra, R. K., Marchon, D., et al. (2017). Nanoparticle decoration with surfactants: Molecular interactions, assembly, and applications. *Surf. Sci. Rep.* 72, 1–58. doi:10.1016/j.surfrep.2017.02.001
- Kango, S., Kalia, S., Celli, A., Njuguna, J., Habibi, Y., and Kumar, R. (2013). Surface modification of inorganic nanoparticles for development of organic-inorganic nanocomposites—a review. *Prog. Polym. Sci.* 38, 1232–1261. doi:10.1016/j.progpolymsci.2013.02.003
- Kargojar, S., Kermani, F., Mollazadeh Beidokhti, S., Hamzehlou, S., Verné, E., Ferraris, S., et al. (2019). Functionalization and surface modifications of bioactive glasses (BGs): Tailoring of the biological response working on the outermost surface layer. *Materials* 12, 3696. doi:10.3390/ma12223696
- Kerschenmeyer, A., Arlov, Ø., Malheiro, V., Steinwachsd, M., Rottmar, M., Maniura-Weber, K., et al. (2017). Anti-oxidant and immune-modulatory properties of sulfated alginate derivatives on human chondrocytes and macrophages. *Biomater. Sci.* 00, 1756–1765. doi:10.1039/c7bm00341b
- Kim, T. H., Singh, R. K., Kang, M. S., Kim, J. H., and Kim, H. W. (2016). Gene delivery nanocarriers of bioactive glass with unique potential to load BMP2 plasmid DNA and to internalize into mesenchymal stem cells for osteogenesis and bone regeneration. *Nanoscale* 8, 8300–8311. doi:10.1039/c5nr07933k
- Kodiyam, A., Silva, E. A., Kim, J., Aizenberg, M., and Mooney D, J. (2012). Surface modification with alginate-derived polymers for stable, protein-repellent, long-circulating gold nanoparticles. *ACS Nano* 6, 4796–4805. doi:10.1021/nn205073n
- Kokubo, T., and Takadama, H. (2006). How useful is SBF in predicting *in vivo* bone bioactivity? *Biomaterials* 27, 2907–2915. doi:10.1016/j.biomaterials.2006.01.017
- Lee, K. Y., and Moone, y. D. J. (2012). Alginate: Properties and biomedical applications. *Prog. Polym. Sci.* 37, 106–126. doi:10.1016/j.progpolymsci.2011.06.003
- Lopez-Noriega, A., Arcos, D., and Vallet-Regi, M. (2010). Functionalizing mesoporous bioglasses for long-term anti-osteoporotic drug delivery. *Chem. Eur. J.* 16, 10879–10886. doi:10.1002/chem.201000137
- Marcos Luciano, B. (2015). *Strategies to modify the drug release from pharmaceutical systems*. Sawston, United Kingdom: Woodhead Publishing, 63–86.
- Meldrum F, C. (2008). Controlling mineral morphologies and structures in biological and synthetic systems. *Chem. Rev.* 108, 4332–4432. doi:10.1021/cr8002856
- Pontremoli, C., Izquierdo-Barba, I., Montalbano, G., Vallet-Regi, M., Vitale-Brovvarone, C., and Fiorilli, S. (2020). Strontium-releasing mesoporous bioactive glasses with anti-adhesive zwitterionic surface as advanced biomaterials for bone tissue regeneration. *J. Colloid Interface Sci.* 563, 92–103. doi:10.1016/j.jcis.2019.12.047
- Rahaman, M. N., Day, D. E., Bal, B. S., Fu, Q., Jung, S. B., Bonewald, L. F., et al. (2011). Bioactive glass in tissue engineering. *Acta Biomater.* 7, 2355–2373. doi:10.1016/j.actbio.2011.03.016
- Ravanbakhsh, M., Labbaf, S., Karimzadeh, F., Pinna, A., Houreh, A. B., and Nasr-Esfahani, M. H. (2019). Mesoporous bioactive glasses for the combined application of osteosarcoma treatment and bone regeneration. *Mater. Sci. Eng. C* 104, 109994. doi:10.1016/j.msec.2019.109994
- Schumacher, M., Habibovic, P., and van Rijt, S. (2021). Mesoporous bioactive glass composition effects on degradation and bioactivity. *Bioact. Mater.* 6, 1921–1931. doi:10.1016/j.bioactmat.2020.12.007
- Schumacher, M., Reither, L., Thomas, J., Kampschulte, M., Gbureck, U., Lode, A., et al. (2017). Calcium phosphate bone cement/mesoporous bioactive glass composites for controlled growth factor delivery. *Biomater. Sci.* 5, 578–588. doi:10.1039/c6bm00903d
- Sharifi, E., Bigham, A., Yousefiasl, S., Trovato, M., Ghomi, M., Esmaeili, Y., et al. (2022). Mesoporous bioactive glasses in cancer diagnosis and therapy: Stimuli-responsive, toxicity, immunogenicity, and clinical translation. *Adv. Sci.* 9, e2102678. doi:10.1002/advs.202102678
- Vallet-Regi, M., and Salinas, A. J. (2021). Mesoporous bioactive glasses for regenerative medicine. *Mater. Today Bio* 11, 100121. doi:10.1016/j.mtbio.2021.100121
- Wang, X., Zeng, D., Weng, W., Huang, Q., Zhang, X., Wen, J., et al. (2018). Alendronate delivery on amino modified mesoporous bioactive glass scaffolds to enhance bone regeneration in osteoporosis rats. *Artif. Cells, Nanomedicine, Biotechnol.* 46, 171–181. doi:10.1080/21691401.2018.1453825
- Xiao, J., Wan, Y., Yang, Z., Huang, Y., Zhu, Y., Yao, F., et al. (2019). Bioactive glass nanotube scaffold with well-ordered mesoporous structure for improved bioactivity and controlled drug delivery. *J. Mater. Sci. Technol.* 35, 1959–1965. doi:10.1016/j.jmst.2019.04.027
- Xiao, J., Wan, Y., Yang, Z., Huang, Y., Zhu, Y., Yao, F., et al. (2019). Simvastatin-loaded nanotubular mesoporous bioactive glass scaffolds for bone tissue engineering. *Microporous Mesoporous Mater.* 288, 109570. doi:10.1016/j.micromeso.2019.109570
- Xu, Y., Wu, P., Feng, P., Guo, W., Yang, W., and Shuai, C. (2018). Interfacial reinforcement in a poly-L-lactic acid/mesoporous bioactive glass scaffold via polydopamine. *Colloids Surfaces B Biointerfaces* 170, 45–53. doi:10.1016/j.colsurfb.2018.05.065
- Yan, H., Chen, X., Bao, C., Wu, S., He, S., and Lin, Q. (2019). Alginate derivative-functionalized silica nanoparticles: Surface modification and characterization. *Polym. Bull. Berl.* 77, 73–84. doi:10.1007/s00289-019-02736-9
- Yan, S., Sun, Y., Chen, A., Liu, L., Zhang, K., Li, G., et al. (2017). Templated fabrication of pH-responsive poly(L-glutamic acid) based nanogels via surface-grafting and macromolecular crosslinking. *RSC Adv.* 7, 14888–14901. doi:10.1039/c7ra00631d
- Yao, H., Zhu, M., Wang, P., Liu, Y., and Wei, J. (2021). Combination of mussel inspired method and “thiol-michael” click reaction for biocompatible alginate-modified carbon nanotubes. *Nanomaterials* 11, 2191. doi:10.3390/nano11092191
- Zhao, D., Zhu, T., Li, J., Cui, L., Zhang, Z., Zhuang, X., et al. (2021). Poly(lactic-co-glycolic acid)-based composite bone-substitute materials. *Bioact. Mater.* 6, 346–360. doi:10.1016/j.bioactmat.2020.08.016
- Zhu, Y., and Stefan, K. (2019). Comparison of the *in vitro* bioactivity and drug release property of mesoporous bioactive glasses (MBGs) and bioactive glasses (BGs) scaffolds. *Microporous Mesoporous Mater.* 118, 176–182. doi:10.1016/j.micromeso.2008.08.046